Building and Environment 267 (2025) 112256

Contents lists available at ScienceDirect

Building and Environment

journal homepage: www.elsevier.com/locate/buildenv

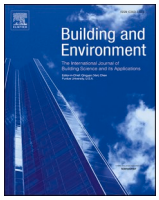

A power-law distribution of infectious quanta for the top 30% of SARS-CoV-2-infected individuals

Pan Cheng [a], Wei Jia [a], Li Liu [c], Hui-Ling Yen [d], Yuguo Li [a,b,*]

[a] Department of Mechanical Engineering, The University of Hong Kong, Hong Kong, China
[b] Faculty of Architecture, The University of Hong Kong, Hong Kong, China
[c] School of Architecture, Tsinghua University, Beijing, China
[d] School of Public Health, The University of Hong Kong, Hong Kong, China

ARTICLE INFO

Key words:
Airborne transmission
Expired droplet
Wells–Riley equation
Population quanta
SARS-CoV-2 outbreak

ABSTRACT

Minimising airborne infection with respiratory viruses, such as SARS-CoV-2, requires knowledge of the infectious quanta generation rate for determining the minimum dilution requirement. The two existing methods for estimating quanta generation rates are the viral load method and outbreak method. The former method is challenged by significant uncertainty in input data, including dose-response parameters and infectious viral loads. The latter method, based on the Wells–Riley equation, is challenged by significant individual heterogeneity in quanta generation rates and lack of outbreak data. In this study, the two methods are integrated for studying the quanta generation profile of all individuals infected with an ancestral SARS-CoV-2 strain, based on four reported outbreaks of infection. The airborne transmission droplet size ranges in the four outbreaks, which were determined in previous studies, are used to estimate the hourly volume of expired droplets for the viral load method. Various viral load datasets and conversion factors from RNA copies to infectious quanta are tested. Two criteria are used to identify the probable quanta generation profile, i.e. 70% of infected individuals do not infect others, and the estimated quanta generation rates estimated using the outbreak method should be within the top 80%–99% of infected individuals. The predicted quanta generation profile of all individuals infected with SARS-CoV-2 follows a log-normal distribution, whereas that of the top 30% of infected individuals approximately follows a power-law distribution.

Practical significance: A major obstacle in defining dilution requirements for minimising airborne infection is the lack of infectious quanta generation rates for the general population. Our approach integrates two existing quanta estimation methods and paves the way to obtaining reliable quanta generation rate profiles at the population level.

1. Introduction

An increasing number of studies have recognised airborne transmission as the predominant route for the spread of respiratory diseases, such as COVID-19 and influenza [18,26,40]. Many studied outbreaks have revealed the long-range airborne transmission of respiratory pathogens such as severe acute respiratory syndrome coronavirus 2 (SARS-CoV-2) [21,25,30], influenza viruses [38], SARS-CoV [17], and Middle East respiratory syndrome coronavirus [41]. Most infections with such respiratory pathogens occur indoors, e.g. infection with SARS-CoV-2 [33]. Respiratory infections can cause death. From 1999 to 2015, an annual seasonal influenza-related respiratory death was estimated at 291,243 – 645,832 [20]. Troeger et al. [35] found that influenza lower respiratory tract infection caused an estimated 145,000 deaths globally in 2017. Lower respiratory infections were ranked as the fourth leading cause of disability-adjusted life-years worldwide in 2019 [39].

Theoretically, airborne infection can be controlled if the released infectious viruses are sufficiently diluted in enclosed spaces. The observation that indoor environments lead to a higher risk of infection than outdoor environments is an indirect but clear piece of evidence [33]. To estimate the minimum dilution required to prevent airborne infection, the infectious quanta generation rates or other infectious units should be known [14,27,34]. An infectious quantum is a quantitative

* Corresponding author at: Department of Mechanical Engineering, The University of Hong Kong, Hong Kong, China.
E-mail address: liyg@hku.hk (Y. Li).

https://doi.org/10.1016/j.buildenv.2024.112256
Received 27 August 2024; Received in revised form 7 October 2024; Accepted 30 October 2024
Available online 31 October 2024

surrogate for an infectious virus unit with a dose–response parameter of unity (1/quantum). Significant individual heterogeneity is expected to exist in quanta generation rates. Most infected individuals do not cause any secondary infection [1]. Superspreading events drive both an initial explosive increase in respiratory infection cases and a sustained transmission of the respiratory pathogen [13]. Ending superspreading events is the key to stopping a pandemic, such as the COVID-19 pandemic, and there is a need to understand individual heterogeneity in virus shedding, differences in susceptibility, and other factors [6]. The degree of individual heterogeneity in quanta generation remains unknown.

Two existing methods for estimating quanta generation rates are the viral load method and outbreak method. The outbreak method, which is based on the Wells–Riley equation, is only applicable to scenarios comprising a specific index case in a particular infection venue. However, the number of outbreaks with sufficient input data for this method is limited. Regarding the viral load method [4,5], viral loads have been widely monitored, and the estimated quanta generation rate profiles may be applicable to the general population, at least theoretically. However, significant uncertainty exists in the conversion factors from RNA copies to infectious quanta and in the viral load datasets. Meanwhile, not all expired droplets contribute to infectious quanta, and the effective size range of expired droplets involved in airborne transmission is a function of the air dilution system ([11,37]; and [31]). In studying the viral load method for determining the population quanta generation rates, Jones et al. [16] concluded that "the predictions are so uncertain that they cannot be used in any meaningful way to provide useful quantitative guidance for designing indoor spaces."

In the present study, the outbreak method based on the Wells–Riley equation and the viral load method are integrated. In the viral load method, a recently obtained volume of hourly generated airborne transmission droplets [11] is tested against three datasets of viral loads and four datasets of conversion factors. In the outbreak method, four outbreaks of infection with the ancestral SARS-CoV-2 strain with full input data are investigated, i.e. a restaurant [21], a courtroom [36], and two buses [30]. The basis for combining the two methods is that the deterministic individual quanta generation rates can be used to evaluate the probabilistic population data. To select the most probable quanta generation rate distribution among those obtained from the viral load method, two criteria are developed, i.e. 70% of infected individuals do not infect others [1], and the quanta generation rates estimated using the outbreak method in the four venues should be within the top 80% – 99% of infected individuals. The minimum quanta generation rate to cause a secondary infection is inferred from existing outbreak data. This novel integrated approach enables us to obtain the first quanta generation rate *distribution* for all infected individuals and for the top 30% of infected individuals.

2. Methods

2.1. Probable quanta generation rate profiles

We define a unit-size bin $[d_b, d_{b+1})$ of expired droplets, where $d_b = 1, 2, 3, 4 \ldots 999$, which is the lower bound of each unit-size bin $[d_b, d_{b+1})$, and $d_{b+1} = d_b + 1$, which is the upper bound of each unit-size bin except when the droplet diameter is <1 μm, i.e. $d_b = 0.1$, $d_{b+1} = 1$. Thus, 1000 unit-size bins exist between 1.0 and 1000 μm and in the range [0.1, 1.0). These bins are all referred to as *unit-size bins*. The bracket notation [) indicates that the lower bound is included in the range, while the upper bound is not.

The expired droplets involved in long-range transmission are referred to as airborne transmission droplets, and their size range is $[d_{o,l}, d_{o,u}]$. All droplets expired from the mouth or nostril within the airborne transmission size range, i.e. airborne transmission droplets, contribute to the infectious quanta generation rate $\dot{Q}$ (number/h). In the viral load method, the quanta generation rate is estimated as follows.

$$\dot{Q} = c_v c_i V_{ex}\big|_{d_{o,l}}^{d_{o,u}}, \tag{1}$$

where $V_{ex}\big|_{d_{o,l}}^{d_{o,u}} = \int_{d_{o,l}}^{d_{o,u}} \frac{dN_{ex}}{d(d_o)} \cdot \frac{\pi}{6} \cdot d_o^3 d d_o$ (mL/h) is the hourly volume of expired droplets within the airborne transmission size range $[d_{o,l}, d_{o,u}]$; c_v (RNA copies/mL) is the viral load in the expired droplets; and c_i (quanta/RNA copies) is the conversion factor from viral RNA copies to infectious quanta.

The viral load c_v is variant-dependent with individual heterogeneity and varies with the number of days after symptom onset. The viral load is assumed to be the same in all droplets. Three datasets of viral loads for the ancestral SARS-CoV-2 strain are tested. The first dataset is from a systematic literature review by Chen et al. [7], which found that $\log_{10} c_v$ follows a Weibull distribution, with a scale factor of 6.66 and a shape factor of 3.52 [$n = 50$] on day 0 after symptom onset, and with other factors on other days after symptom onset. The second dataset is from the study by Puhach et al. [32], who identified 15 samples of the ancestral SARS-CoV-2 strain and detected 13 of them to have non-zero values of focus-forming units. The log10-transformed viral load results of the 13 samples [$n = 13$] are fitted with a normal distribution of $N(8.85,\ 1.18^2)$ in the present study (Supplementary Information SI 1). Additionally, the datasets from the study by Buonanno et al. [4] were also tested but were not found to satisfy our criteria. Buonanno et al. [4] considered a normal distribution of $N(7,\ 0.71^2)$ for $\log_{10} c_v$ with reference to five viral load datasets in the literature.

Four datasets of the conversion factor c_i are identified. The first three are as follows: a value within the range of 0.01–0.10 (denoted 'uniform'; [5]); a constant value of 1/700 (denoted 'constant'; [3]); and a revised constant value of 0.0146 (denoted 'constant', identified in this study). The proposal of the revised constant value ($c_i = 0.0146$) will be explained later in Section 2.4. Buonanno et al. [5] did not specify the distribution for the conversion factor c_i, so a uniform distribution $U(0.01,\ 0.1)$ is assigned in this study. Fourthly, the reciprocal of the product of two normal distributions, $N(210,\ 21^2)$ and $N(130,\ 13^2)$, from the study by Buonanno et al. [4] was tested, but was not found to be suitable.

Finally, with two chosen datasets for the viral load c_v and three chosen datasets for the conversion factor c_i, we have six possible combinations of viral load and conversion factor for estimating quanta generation. The built-in function of the empirical cumulative distribution function plot (cdfplot) is used to obtain the cumulative probability mass plots for c_v and c_i (Figure S1.1).

Each combination of input data generates a quanta generation rate profile. Choosing the most probable profile is not an easy task. A probability distribution is characterised by both location and scale parameters (Fig. 1). The location of the probability distribution is determined using the observation that 70% of infected individuals did not cause any secondary infection. There is a need to determine the corresponding quanta threshold value $\dot{Q}_{70\%}$ at which no infection occurs. The shape of a probability distribution is guided by the spread of the curve. Our strategy is to use the quanta generation rates from the observed outbreaks. Ideally, if the sample size is sufficient, such a strategy should work well. Only the curves within the range of the known quanta generation rates are possible candidates. The challenge is that the number of outbreaks with reliable input data is limited. The detailed selection strategy is described later in Sections 2.4 and 2.5.

2.2. Four infection venues

A major input parameter in the viral load method is the hourly volume of expired droplets within the airborne transmission droplet size range $[d_{o,l}, d_{o,u}]$. The airborne transmission droplet size range may not be identical in all spaces, but instead depends on dilution ability. Hypothetically, with a 'typhoon' wind in a building, no expired droplets

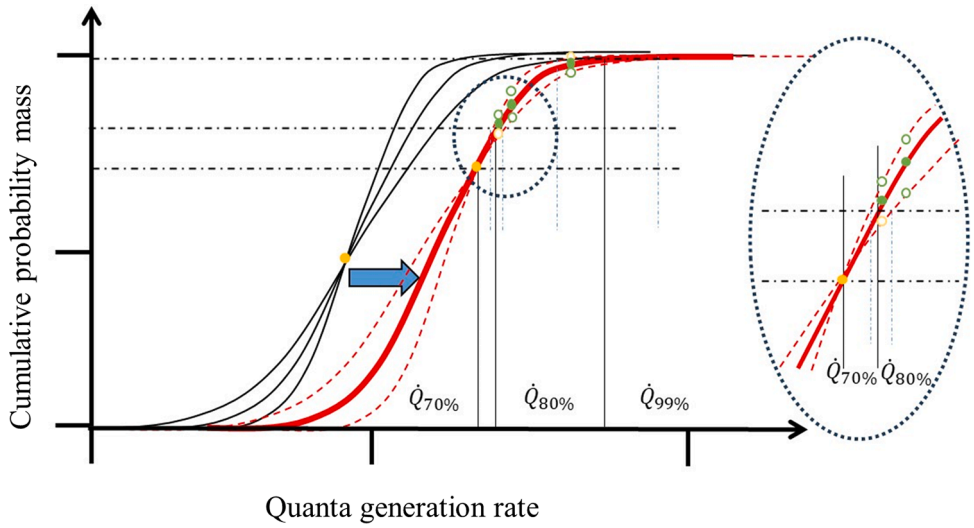

Fig. 1. Screening criteria for determining the shape and location of the cumulative probability distribution of the population quanta generation rates.

would be able to be airborne, but would instead be completely removed so that the range of droplet sizes involved would be zero. It is thus essential to use a realistic range of dilution flow rates to estimate [$d_{o,l}$, $d_{o,u}$].

We examined four venues of COVID-19 outbreaks for which approximately complete outbreak and environmental data are available: a courtroom, a restaurant, and two buses (Table 1). In all four outbreaks, exposure occurred on the day of symptom onset of the index case, and the outbreaks were caused by the ancestral SARS-CoV-2 strain. The outbreaks exhibited varying levels of attack rates (10.2% to 33.3%), occupied air volumes (1.2 to 15.0 m^3 per person), ventilation rates (0.9 to 3.5 L/s per person), total dilution (3.52 to 7.60 L/s per person), and exposure time (1.0 to 3.3 h).

The exhalation and inhalation rates are estimated based on metabolic rates, which are in turn estimated from the observed physical and respiratory activities. The exhalation and inhalation rates are similar across all venues except the restaurant, where the index case exhibited a high level of body movement and vocalisation, resulting in an increased pulmonary rate.

In our previous study [11], we estimated the airborne transmission droplets in the four outbreak venues using the droplet dataset provided by Johnson et al. [15]. The dataset covered the range of 0.1–30 μm for breathing and 0.1–1000 μm for speaking. Using $\frac{dN_{ex}(d_o)}{dd_o} = \frac{dC_{ex}(d_o)}{dd_o} q_{ex}$, we estimated the size distribution of expired droplets. A transient number balance model was used together with existing formulas for size-resolved settling rates and filtration efficiencies, and a deposition model from the International Commission on Radiological Protection. This enabled a determination of the size-resolved concentrations of exhaled droplets in indoor air, the size-resolved number of droplet nuclei in the inhaled air, and the number of droplets deposited throughout the respiratory tract.

Three criteria were used to determine whether a droplet unit-size bin should be included in airborne transmission droplet size range [11]. The first criterion is the *indoor air criterion*, i.e. the number concentration within that bin at the steady state must be equal to or greater than 1 #/m^3. The second criterion is the *inhalation criterion*, i.e. at least one

Table 1
Outbreak-related data for the four COVID-19 outbreak venues (adapted from [11]). The quanta generation rates in bold are calculated using the dilution flow rates in the table, and those in normal font are obtained from the literature.

Parameter category	Parameter	Courtroom	Restaurant	Bus 1	Bus 2
Studies		Vernez et al. [36]	Li et al. [21]	Ou et al. [30]	Ou et al. [30]
	Exposure date[a]	09/30	01/24	01/22	01/22
	Symptom onset date[a]	09/30	01/24	01/22	01/22
	Day from symptom onset to transmission	0	0	0	0
Outbreak	No. of index cases	1	1	1	1
	No. of susceptible individuals	9	88	46	17
	No. of secondary infections	3	9	7	2
	Attack rate (%)	33.3	10.2	15.22	11.76
Venue	Air volume (m^3)	150	431	60.42	21.69
	Occupancy (m^3 per person)	15.0	4.8	1.3	1.2
Room dilution (h^{-1}, or L/s)[b]	Total dilution, q_T	55.0	677.6	96.2	63.4
	Transient correction factor ($1 - C_t$)	0.75	0.85	0.95	0.90
Dilution per person (L/(s·person))[b]	Outdoor air, q_v	1.62	0.90	1.71	3.21
	Total dilution, q_t	5.50	7.60	2.05	3.52
Pulmonary rate and exposure	Inhalation rate[c], q_{in}, m^3/h	0.576	0.701	0.576	0.576
	Average exposure time Δt, h	3.0	1.206	3.33	1.0
	Mask wearing	None	None	None[d]	None[d]
Targeted quanta generation rate $\dot{Q}$ (quanta/h)		**61.7**–90.0	154.9–**364.6**	**31.4**–37.1	**54.8**–65.9

[a] The outbreak occurred in 2020.
[b] The settling rate is assumed to be a constant of 0.3 h^{-1}. The filtration efficiency in the restaurant is 20% [21].
[c] The inhalation rate q_{in} and the exhalation rate q_{ex} are assumed to be equal and are estimated based on observed activities [11].
[d] Only five passengers on Bus 1 and one passenger on Bus 2 were found to be wearing masks based on the available screenshots from closed-circuit television videos [30]. Mask wearing is not considered in the calculations.

particle (droplet) in a unit-size bin $[d_b, d_{b+1})$ must be inhaled within the exposure duration. The third criterion is the *deposition criterion*, i.e. at least one particle (droplet) within a unit-size bin must be deposited in the total respiratory tract within the exposure duration. The size range determined by the inhalation criterion is always the largest, which is chosen for this study. For the courtroom, the size range is [0.1, 6]; for the restaurant, it is [0.1, 4]; and for Bus 1 and Bus 2, it is [0.1, 5]. The hourly numbers (volumes) of expired droplets are 95,043.4 #/h (0.40 nL/h) in the courtroom, 113,111.8 #/h (0.42 nL/h) in the restaurant, and 96, 320.1 #/h (0.38 nL/h) on the buses. The volume of the hourly generated airborne transmission droplets does not vary significantly with the determined size range, when the upper/lower bound of the 95% confidence interval and the average size distribution of the expired droplets are employed respectively [11].

2.3. Targeted quanta generation rates

For consistency, a set of quanta generation rates $\dot{Q}$ is estimated from the reported outbreaks using the transient Wells–Riley equation.

$$P = 1 - e^{-\dot{Q}\frac{q_{in}}{q_d}\Delta t(1-C_t)} \tag{2}$$

where P is the observed attack rate in the outbreak, and q_d is the total dilution rate obtained using settling/filtration data in each of the outbreak venues, L/s. The index case arrives at time $t = 0$, and Δt is the exposure duration in hours. Regarding the transient effect, the coefficient $C_t = \frac{1-e^{-n_T\Delta t}}{n_T\Delta t}$ is the transient correction factor, where n_T is air changes per hour. The total dilution rates and inhalation rates provided in Table 1 are used, and the targeted quanta generation rates are also summarised in Table 1, which are obtained as follows.

For the courtroom, a transient Wells–Riley model gives a quanta generation rate of 61.7 quanta/h using the total dilution data in Table 1. Vernez et al. [36] estimated a mean value of 90.0 quanta/h when the ventilation rate was 0.23/h and the windows were closed. They conducted Monte Carlo simulations with an infection probability of $\frac{3}{9}-\frac{4}{9}$ and a settling rate of $0.3-1.5$, whereas only the lower ends of the two parameters, $\frac{3}{9}$ and 0.3, are used in our calculations. Considering uncertainties, the targeted quanta generation rate falls into the range of 61.7–90.0 quanta/h for the courtroom.

For the restaurant, the transient Wells–Riley model gave quanta generation rates of 79.3 quanta/h in the study by Li et al. [21] and 154.9 quanta/h in the study by Jia et al. [14] (in which the restaurant was considered as a single zone) and a quanta generation rate of 364.6 quanta/h using the total dilution data in Table 1. Li et al. [21] did not consider the dilution caused by filtration and assigned an inhalation rate of 1.65 m^3/h to the occupants, which led to a low prediction of the quanta generation rate. Jia et al. [14] considered filtration but still assigned a high inhalation rate (1.65 m^3/h) to the occupants and thus obtained a mid-level quanta generation rate. Here, an inhalation rate of 0.701 m^3/h is estimated, and filtration is accounted for. The targeted quanta generation rates for the restaurant fall into the range of 154.9–364.6 quanta/h.

For Buses 1 and 2, Cheng et al. [9] determined the quanta generation rates of 37.1 and 65.9 quanta/h, respectively. Ou et al. [30] adopted a steady-state Wells–Riley equation and estimated 35.0 quanta/h for Bus 1 and 58.3 quanta/h for Bus 2 (or 36.9 and 64.4 quanta/h, respectively, when a transient equation was used). In the current study, the inhalation rate of 0.576 m^3/h yields slightly lower quanta generation rates of 31.4 and 54.8 for Buses 1 and 2, respectively, than the inhalation rate of 0.49 m^3/h used by Cheng et al. [9] and Ou et al. [30]. The targeted quanta generation rates for Buses 1 and 2 fall into the ranges 31.4–37.1 and 54.8–65.9 quanta/h, respectively.

2.4. Threshold quanta generation rate for locating the probability distribution

The steady-state Wells–Riley equation for one infector in a venue states that $P = \frac{N_s}{N_\sigma} = 1 - e^{\left(-\dot{Q}\frac{q_{in}}{q_T}\Delta t\right)}$, where N_σ is the number of susceptible individuals, q_T is the total dilution air flow rate (m^3/h), and $\dot{Q}$ is the quanta generation rate (quanta/h). The exposure time Δt is usually one to a few hours in most indoor venues, such as classrooms, restaurants, and buses. When the infection probability is sufficiently small, the equation can be simplified as $P \approx \dot{Q}\frac{q_{in}}{q_T}\Delta t$. Consequently, the number of secondary cases can be approximated as $N_s = \dot{Q}\frac{q_{in}\Delta t}{q_t}\frac{N_\sigma}{N_\sigma+1}$, where $q_t\left(=\frac{q_T}{N_\sigma+1}\right)$ is the dilution rate per person and $\frac{N_\sigma}{N_\sigma+1}$ is less than 0.9 when $N_\sigma < 9$. If $\dot{Q} > \frac{q_t}{q_{in}\Delta t}\frac{N_\sigma+1}{N_\sigma}$, $N_s > 1$. This means that if the 'average' dilution rate per person, the 'average' exposure time and the average number of susceptible individuals are all known, the threshold quanta generation rate for producing one secondary infection can be estimated.

Adam et al. [1] identified 169 resolved COVID-19 transmission pairs of infector–infectee in Hong Kong during the period from 23 January 2020 to 28 April 2020 and found that 69% (65%–71%) of cases did not transmit to others. This allows us to suggest a criterion for the location of the probability curve (Fig. 1), i.e. at 70%, the quanta generation rate should be the threshold quanta generation rate.

There are at least two methods to obtain the average dilution rate and average exposure time. The first is to obtain the typical dilution flow rates and people's gathering time in a sufficient number of indoor spaces across the 'world'. Such data are not available yet. It is also likely that many indoor spaces do not lead to secondary infections. The second is to gather data from observed outbreaks. Here we use COVID-19 outbreaks as an example. Luo et al. [22] identified 50 COVID-19 outbreaks, and 13 of these have available or estimated dilution rates (SI 2). These 13 outbreaks are summarised in Table S2.1. The mean equivalent dilution rate q_t is 9.14 L/s per person. The mean exposure time is 4.16 h The average number of susceptible individuals is 140. The estimated inhalation rates q_{in} for occupants (sitting, occasionally speaking) range from 0.15 to 0.20 L/s. The corresponding threshold quanta generation rates in these venues range from 11.06 to 14.75 quanta/h, with an average of 12.91 quanta/h, i.e. at most one secondary infection occurs ($N_s \leq 1$). Therefore, a threshold quanta generation rate of 13 quanta/h is established.

Aeroplanes are expected to be mostly well diluted, and the inclusion of aeroplanes may distort the dilution data of typical indoor spaces on land. Therefore, after excluding the aeroplane outbreaks, the mean equivalent dilution rate q_t is 5.09 L/s per person and the mean exposure time is 1.79 h The average number of susceptible individuals is 72. The corresponding threshold quanta generation rates of these venues range from 14.37 to 19.16 quanta/h, with an average of 16.76 quanta/h. Thus, another threshold quanta generation rate of 17 quanta/h is found.

For simplicity and considering uncertainty, the chosen 70th percentile value is 17 quanta/h in this study. The revised constant value of 0.0146 is proposed to meet the criterion: $\dot{Q}_{70\%} = 17$ quanta/h for the Puhach et al. [32] viral load dataset. For the other two viral load datasets, conversion factors higher than 1 ($c_i = 2.04$ and $c_i = 3.40$, respectively) are required to achieve $\dot{Q}_{70\%} = 17$ quanta/h, and thus are not considered. Calculations are also performed for a value of 13 quanta/h (SI 3). Similarly, a revised constant value of 0.0111 is proposed to meet the criterion: $\dot{Q}_{70\%} = 13$ quanta/h for the Puhach et al. [32] viral load dataset. For the other two viral load datasets, conversion factors higher than 1 ($c_i = 1.56$ and $c_i = 2.60$, respectively) are required to achieve $\dot{Q}_{70\%} = 13$ quanta/h, and thus are not considered.

2.5. Strategy for selecting the shape of the quanta probability distribution

Adam et al. [1] also estimated that '19% (15%–24%) of cases were responsible for 80% of all SARS-CoV-2 transmission in Hong Kong', which follows the 20/80 rule. We infer that the quanta generation rates for the index cases in the observed outbreaks should be within the top 20% of infected individuals. The number of secondary infections in each outbreak caused by an infected individual between the top 30% and top 20% of infected individuals is likely to be small, and such outbreaks are probably less likely to be identified than those caused by the top 20% infected individuals.

We further assume that the quanta generation rates for the index cases in the observed outbreaks should be within the 80th–99th percentile range. The 99th percentile upper limit is laid artificially to avoid the randomness and rareness of extremely high quanta generation rates in the population. To demonstrate how the quanta generation rates from the outbreaks can be used to select the shape of the quanta probability curve, consider three curves that satisfy the location criterion (Fig. 1). The curve that is 'narrower' than the middle curve (thick solid line in red) has one quanta value located beyond the 99th percentile, so it is not chosen. The curve that is 'wider' than the middle curve has one quanta value located between 70% and 80%, so it is also not chosen.

3. Results

3.1. The viral load dataset published by Puhach et al. [32] and a revised constant conversion factor ($c_i = 0.0146$) yield the most appropriate $\dot{Q}$ distribution

For the four outbreaks studied here, each had a single index case, and virus transmission in all of the outbreaks occurred on the first day of the index cases' symptom onset. This allows us to estimate the quanta emission rate for each index case on the first day of symptom onset.

A significant heterogeneity in the viral load is expected between individuals. This suggests that it is impossible to use the viral load approach to predict the exact viral load profile of an individual on a particular day. Moreover, the number of expired droplets exhibits heterogeneity.

Fig. 2 illustrates how we arrive at the quanta emission rate profile determined using the viral load dataset provided by Puhach et al. [32] and a revised constant conversion factor (0.0146). For all four outbreaks, only one such combination, i.e. 'Puhach–revised constant', enables the target quanta emission rates to fall within the 80th–99th percentile ranges and also satisfies the location requirement of the 70% quanta value of 17 quanta/h. Hence, only the 'Puhach–revised constant' quanta profile is retained. However, the targeted quanta value (31.4–37.1 quanta/h) for Bus 1 is slightly lower than the $\dot{Q}_{80\%}$ to $\dot{Q}_{99\%}$ range (Fig. 3), and is reluctantly accepted here considering the uncertainty in input data in the outbreak.

A total of 24 quanta generation rate profiles are summarised in Table 2 for the four outbreaks, with each outbreak analysed using six combinations of viral load and conversion factor.

3.2. The quanta generation profiles of the top 30% of infected individuals follow a power-law distribution

The quanta generation rate profiles that are estimated using the combination 'Puhach–revised constant ($c_i = 0.0146$)' are relatively consistent across the four venues, even though these venues had different dilution abilities. The complete quanta generation profiles are found to follow a log-normal distribution (Fig. 4), i.e. $\log_{10}\dot{Q} \sim N(0.62,\ 1.18^2)$ for the courtroom, $N(0.64,\ 1.18^2)$ for the restaurant, and $N(0.59,\ 1.18^2)$ for the buses. The adjusted R^2 values are near 1 for all, showing that the fitted parameters estimate almost 100% of the variation in the dataset. The log-normal distribution seems to capture well the spread and central tendency of the quanta generation rates for the population infected with the ancestral SARS-CoV-2 strain, with most values clustering around a central value, but also having a long tail towards larger values.

The probability of each quanta generation rate for the top 30% of infected individuals for the investigated venues, i.e. $P(N) = \int_{N-0.5}^{N+0.5} f(\dot{Q})d(\dot{Q})$, is shown in Fig. 5. All of the estimated probability profiles follow a power-law distribution, i.e. $P(N) = 0.351N^{-1.341}$ for the courtroom, $P(N) = 0.359N^{-1.342}$ for the restaurant, and $P(N) = 0.345N^{-1.341}$ for the two buses. The closest natural numbers to the 70th percentile value (17 for the courtroom, 18 for the restaurant, and 16 for the buses) are used as the starting point of the fitting dataset.

The hourly volume of expired droplets in the long-range airborne transmission size range is 0.40 nL/h for the courtroom, 0.42 nL/h for the restaurant, and 0.38 nL/h for the buses. Considering the average hourly volume of 0.395 nL/h across the four outbreak venues, the estimated probability profiles of the top 30% of quanta generation rates follow a power-law distribution as $P(N) = 0.352N^{-1.343}$. The full list of probabilities of the final quanta generation rates between 0 quanta/h and 1000 quanta/h is attached. Please refer to the Excel file named Probability_Power law.xls.

4. Discussion

4.1. The power-law distribution of the quanta generation rates partially explains the superspreading events

Our study is the probably first to demonstrate that the quanta generation rates for the top 30% of infected individuals follow a power-law distribution.

Many studies on super-spreading events (e.g. [1]) have suggested that the top 20% of infected individuals are responsible for most secondary infections and that the bottom 70% of infected individuals do not infect anyone. It is thus essential to determine the distribution of the quanta generation rates for the top 20%–30% of the population (Fig. 3). It may not be a coincidence that our estimated data show that up to approximately 80% of infected individuals have quanta generation rates of less than ~40 quanta/h. Our approach uses various combinations of input data, specifically viral loads and conversion factors. Multiple quanta generation rate profiles are predicted. We have used the observed characteristics of superspreading events and the outbreak data to choose the most likely quanta profile. Our finally obtained quanta generation profile satisfies the observation that the bottom 70% of infected individuals do not infect anyone ($\dot{Q} < 17$ quanta/h). Moreover, the top 20% of infected individuals cause most of the secondary infections, that is, the quanta generation rates obtained from existing outbreaks are within the top 20% of infected individuals.

This is the first study to obtain the first complete profile of quanta generation rates of the top 30% of infected individuals. Further verification of this profile will enable it to be used to develop minimum dilution requirements for respiratory infection control. The quanta generation rate of the top 30% of infected individuals follows a power-law distribution, whereas that for all infected individuals follows approximately a log-normal distribution. Such a power-law distribution of the top 30% of infected individuals may explain why super-spreading events follow a power-law or negative binomial distribution [1].

In the classical Wells–Riley equation, if infectious quanta generation rates are known, the dilution required to reduce the infection risk to an acceptable level may be determined in any setting [27]. This is only theoretically correct. The infectious quanta generation rate profile of the general infected population is needed, rather than that of a particular index case at an outbreak venue. The latter is only applicable to a specific index case in a specific setting. The population quanta generation rates should be used to determine the minimum dilution rates. However, the existence of super-emitters suggests that no minimum dilution rate

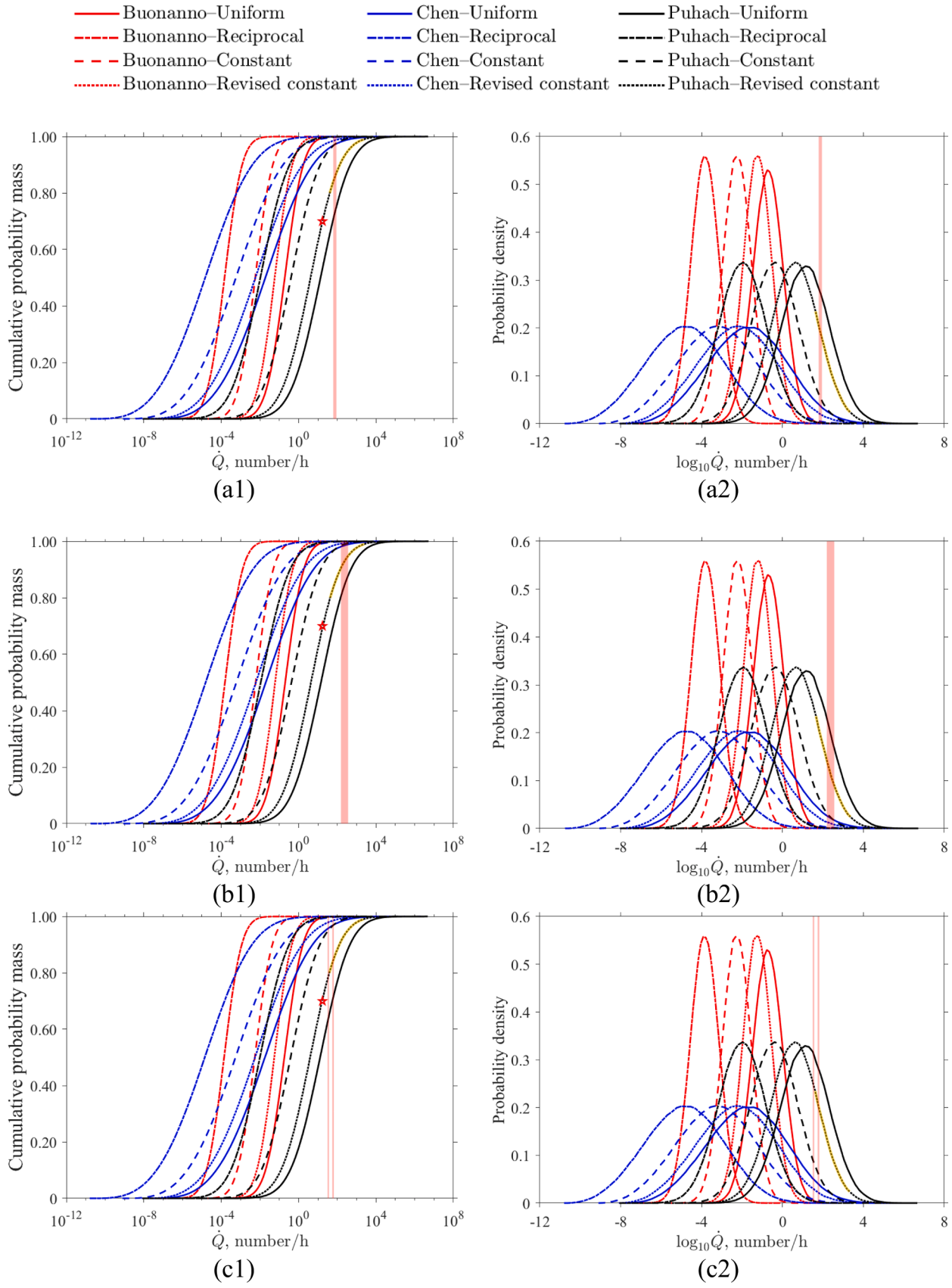

Fig. 2. (a1–c1): The cumulative probability mass $\int_{(\dot{Q})_{min}}^{\dot{Q}} f(\dot{Q})d(\dot{Q})$, from the minimum value $\dot{Q}_{min}$ to $\dot{Q}$ of interest; (a2–c2): The probability density $f(\log_{10}\dot{Q})$ as a function of $\log_{10}\dot{Q}$ for the courtroom, the restaurant, Bus 1, and Bus 2, where the target $\dot{Q}$ ranges are shown by a translucent band in red. Two bands are shown in (c1) and (c2) for Buses 1 and 2, respectively. The red star indicates point (17, 0.7), while the golden curve highlights the range $[\dot{Q}_{80\%}, \dot{Q}_{99\%}]$ in the selected profile.

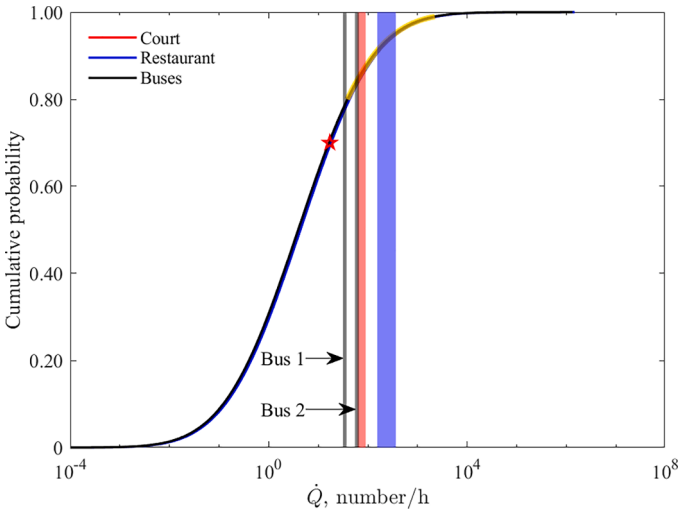

Fig. 3. The $\int_{(\dot{Q})_{min}}^{\dot{Q}} f(\dot{Q})d(\dot{Q})$ curves for the four outbreaks, i.e. the cumulative probability mass, obtained using the viral load dataset reported by Puhach et al. [32] and a revised constant conversion factor (0.0146). The transparent red band represents the target quanta generation rates for the courtroom (61.7–90.0 quanta/h), blue for the Guangzhou restaurant (154.9–364.6 quanta/h), left black band for Bus 1 (31.4–37.1 quanta/h), and right black band for Bus 2 (54.8–65.9 quanta/h). The red star indicates the point (17, 0.7), while the golden curve highlights the profile from the $\dot{Q}_{80\%}$ to $\dot{Q}_{99\%}$ range in the selected percentile.

exists for any single space to avoid infection. For example, for a quanta generation rate of 100 quanta/h and exposure time of 1 h, a dilution air flow rate larger than 10 L/s per person might be sufficient in a large classroom to avoid a secondary infection. However, for a quanta generation rate of 2000 quanta/h (Table 2), a dilution air flow rate larger than 200 L/s per person will be needed, which is unrealistically high for typical classroom settings. A population strategy should be used to control the spread of pathogen in an epidemic or pandemic of airborne infection. The causes of superspreading events are not limited to super-emitters. Super-contactors (with close contacts to many susceptible persons), super-exposure (long exposure time), and poorly ventilated spaces are also possible causes. It might be possible to develop dilution strategies at the building stock scale to ensure that the population reproduction number R0 is less than one. This will require a knowledge of the dilution air flow rate profiles of the building stock in a city, the exposure time distribution in different indoor settings in a city and their metabolic activity profiles. The eventual implementation of such dilution measures needs to consider trade-offs between health, comfort, energy, and cost [12].

The quanta generation rate for the total infected population is found to follow a log-normal distribution. The top 30% infected is a fraction of the infected population, and the quanta generation rate profile for the top 30% is the right tail of the log-normal distribution of the total population. The right tail is very important to infection control. Both log-normal distribution and power-law distribution would imply that the top infected individuals have high quanta generation rates. It is unfortunate there is a lack of the observed high quanta generation rate data at the very right tail for verification. A lognormal distribution would predict a higher quanta generation rate at its right tail and a

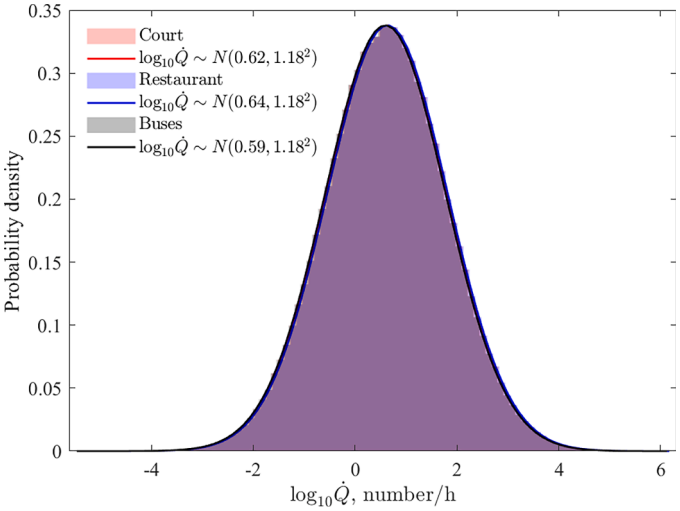

Fig. 4. $(\log_{10}\dot{Q})$: probability density around $\log_{10}\dot{Q}$ of interest, comparing the estimated and fitted distributions of $\log_{10}\dot{Q}$ for the courtroom, restaurant, and two buses. The shaded areas under the fitted curves are of a mixed colour due to the overlapping of red, blue, and black.

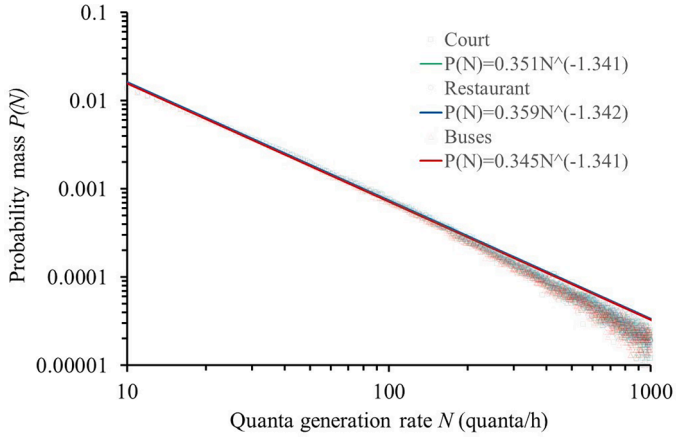

Fig. 5. Probability of each quanta emission rate having certain values: $P(N) = \int_{N-0.5}^{N+0.5} f(\dot{Q})d(\dot{Q})$, where N is a natural number higher than the 70th percentile values in each venue.

Table 2
Comparison between the target ranges and the estimated $\dot{Q}_{80\%}$ to $\dot{Q}_{99\%}$ ranges in the four outbreaks using six combinations of viral load and conversion factor.

Venue	Target range	Chen–uniform	Chen–constant (1/700)	Chen–revised constant (0.0146)
Courtroom	61.7–90	**0.8–391.3**	0.0–10.7	0.2–109.4
Restaurant	154.9–364.6	**0.9–410.9**	0.0–11.3	0.3–114.9
Bus 1	31.4–37.1	**0.8–371.7**	0.0–10.2	0.2–103.9
Bus 2	54.8–65.9	**0.8–371.7**	0.0–10.2	0.2–103.9
Venue	Target range	Puhach–uniform	Puhach–constant (1/700)	Puhach–revised constant (0.0146)
Courtroom	61.7–90	140.0–8714.6	4.0–230.3	**40.7–2348.8**
Restaurant	154.9–364.6	147.0–9150.3	4.2–241.8	**42.7–2466.2**
Bus 1	31.4–37.1	133.0–8278.9	3.8–218.8	**38.6–2231.3**
Bus 2	54.8–65.9	133.0–8278.9	3.8–218.8	**38.6–2231.3**

power-law distribution predicts less. For example, in the considered restaurant, our Monte Carlo simulation using the integrated method predicts a quanta generation rate of 2470 quanta/h for the 99th percentile infected, while the fitted log-normal distribution predicts a corresponding value of 2420 quanta/h, and the power-law distribution predicts 1223 quanta/h.

The underlying mechanisms for the observed quanta generation rate distribution remain to be studied. The quanta generation rates would depend on a number of multiplicative factors (Eq. (1)), i.e. the number and size of the airborne transmission droplets (considered to be constant in our study), the viral load (log-normal or normal distribution), the conversion factor from RNA copies to infectious quanta or the dose-response parameter (depends on the susceptible persons in terms of susceptibility and immunity, distribution unknown) etc. Multiplicative products of random factors are known to be log-normal [24]. If the viral load is the major determining factor (very likely), then the viral load itself and the susceptibility of the population are both heterogeneous (e.g. for example see [29]).

This study represents likely the first attempt to obtain a quanta generation distribution at the population level with verification by outbreak data and infection data. Quanta generation rates may also be obtained for different days after symptom onset by using available viral load data (e.g. [7]). Data on transmissivity could be used to derive infectious quanta generation profiles for different variants of SARS-CoV-2.

4.2. The new profile selection method offers a new approach for determining the population-level quanta generation rates

The viral load method first developed by Buonanno et al. [4] differs from the outbreak method and has one obvious advantage in that it requires no outbreak-related data. The outbreak method requires exact dilution parameters inside the venue, such as the ventilation rate and filtration rate, at the time of exposure. However, ventilation rates often vary in time, depending on window/fan use and air conditioning operation, and it is not straightforward to access an outbreak venue to measure ventilation or other types of dilution and collect detailed associated infection data. There have likely been millions of outbreaks of SARS-CoV-2 infection worldwide, but complete dilution monitoring has been conducted only for a very small number of these outbreaks; in fact, to the best of our knowledge, complete dilution monitoring has only been performed for the four outbreaks studied here and two other restaurant outbreaks in Hong Kong [8]. Furthermore, in the case of many outbreaks, such as the Luk Chuen House outbreak in Hong Kong [10], it is difficult to determine the exposure time. It is difficult to collect data on enough outbreaks (i.e. a sufficient sample size) to determine the infectious quanta generation rate distribution using the outbreak method.

The viral load method of estimating infectious quanta generation rates for the general population requires three datasets, namely datasets of the expired droplet size distribution within the airborne size range, viral load distribution, and conversion factors from the viral load to infection quanta. The size-dependent settling rate [28] and filtration efficiency are essential for estimating the airborne droplet size range for airborne transmission. The existing conversion factors contain significant uncertainty [4]. Thus, a major contribution of the current study in terms of methodology is its integration of the outbreak method and major transmission characteristics into the viral load method developed by Buonanno et al. [4]. Our novel profile selection method (for both location and shape selection) partly resolves the lack of data on the conversion factor and the uncertainty in viral load distribution. Our developed method should be applicable to other respiratory infections which are predominantly transmitted by the airborne route, particularly those with significant individual heterogeneity [19] as with SARS-CoV-2. However, both outbreak data and infection data are needed for choosing the shape and location parameters in the quanta generation rate profiles. Our obtained profile might need to be adjusted using local heterogeneity data of infection. We used the 80/20 rule of Adam et al. [1]. Similar results were obtained elsewhere (e.g. [2]). In Marks et al. [23] studied a cohort of 282 index cases, and found that 68% did not cause secondary infections, while 32% caused infection clusters.

Our study also demonstrates a need to obtain reliable data on the expired droplet profiles of the infected individuals, the viral load profiles, and conversion factors from RNA copies to infectious quanta, as all three of these parameters exhibit high heterogeneity across individuals and activities.

4.3. Limitations

This study has several limitations. First, the accuracy of our estimates of infectious quanta generation rates depends on the accuracy of the available data on expired droplets, viral load, conversion factor, and dilution flow rates. As more accurate data become available, our developed approach can be used to refine the estimates. However, our proposed location and shape selection method shows promise in handling some aspects of data uncertainty.

Second, the sample size for the outbreak data is too small for determining the threshold quanta generation rate for location selection. Additionally, only data from four outbreak venues are used for shape selection. Availability of more outbreak data will further improve the selection. For outbreak investigations, we suggest implementing a more comprehensive and standardized reporting system that includes the environmental measurement such as ventilation and filtration. Low-cost hourly indoor air quality monitoring might be installed in targeted indoor spaces such as nursing homes, restaurants and jails etc. as infection hotspots, so that when an outbreak occurs in one of such monitored spaces, the environmental data can be retrieved. New privacy-proof technologies for monitoring occupancy and close contacts may also be used [42].

Third, our determination of the quanta generation rate is limited to the ancestral SARS-CoV-2 strain and the day of symptom onset. The developed method may be extended to other respiratory viruses and the full course of the disease. In an upcoming study, this was achieved using the quanta generation rate profile in this study, together with relative transmissivity and infectivity data from the literature.

5. Conclusion

Stopping superspreading events is the key to ending a pandemic such as the COVID-19 pandemic. The knowledge of the quanta generation profile of the infected population is essential for understanding superspreading events. The viral load method originally developed by Buonanno et al. [4] suggests that it should be possible to estimate quanta generation rates on a population level, but a reliable profile of quanta generation rates has not been obtained due to the significant uncertainty in input data. The profile is obtained in this study using a novel location and shape selection method that requires the observed outbreak data and the transmission characteristics. The predicted quanta generation profile of the infected individuals with ancestral SARS-CoV-2 follows a log-normal distribution, whereas that of the top 30% of infected individuals approximately follows a power-law distribution. Our obtained quanta generation profile of the top 30% of SARS-CoV-2-infected individuals can be used to determine the minimum dilution required to minimise or avoid infection.

CRediT authorship contribution statement

Pan Cheng: Writing – review & editing, Writing – original draft, Validation, Investigation, Formal analysis, Data curation. **Wei Jia:** Writing – review & editing, Data curation. **Li Liu:** Writing – review & editing, Data curation. **Hui-Ling Yen:** Writing – review & editing, Validation, Data curation, Conceptualization. **Yuguo Li:** Writing – review & editing, Writing – original draft, Supervision, Resources,

Methodology, Conceptualization.

Declaration of competing interest

The authors declare that they have no known competing financial interests or personal relationships that could have appeared to influence the work reported in this paper.

Acknowledgements

This work was supported by the Research Grants Council of Hong Kong's Collaborative Research Fund (grant number C7104–21G) and a General Research Grant (grant number 17206522). Professional English-language editing support was provided by AsiaEdit (asiaedit.com).

Supplementary materials

Supplementary material associated with this article can be found, in the online version, at doi:10.1016/j.buildenv.2024.112256.

Data availability

Data will be made available on request.

References

[1] D.C. Adam, P. Wu, J.Y. Wong, E.H.Y. Lau, T.K. Tsang, S. Cauchemez, et al., Clustering and superspreading potential of SARS-CoV-2 infections in Hong Kong, Nat. Med. 26 (11) (2020) 1714–1719.
[2] T.L. Anderson, A. Nande, C. Merenstein, B. Raynor, A. Oommen, B.J. Kelly, et al., Quantifying individual-level heterogeneity in infectiousness and susceptibility through household studies, Epidemics. 44 (2023) 100710.
[3] M. Bertone, A. Mikszewski, L. Stabile, G. Riccio, G. Cortellessa, F.R. d'Ambrosio, et al., Assessment of SARS-CoV-2 airborne infection transmission risk in public buses, Geosci. Front. 13 (6) (2022) 101398.
[4] G. Buonanno, L. Morawska, L. Stabile, Quantitative assessment of the risk of airborne transmission of SARS-CoV-2 infection: prospective and retrospective applications, Environ. Int. 145 (2020) 106112.
[5] G. Buonanno, L. Stabile, L. Morawska, Estimation of airborne viral emission: quanta emission rate of SARS-CoV-2 for infection risk assessment, Environ. Int. 141 (2020) 105794.
[6] P.Z. Chen, M. Koopmans, D.N. Fisman, F.X. Gu, Understanding why superspreading drives the COVID-19 pandemic but not the H1N1 pandemic, Lancet Infect. Dis. 21 (9) (2021) 1203–1204.
[7] P.Z. Chen, N. Bobrovitz, Z. Premji, M. Koopmans, D.N. Fisman, F.X. Gu, Heterogeneity in transmissibility and shedding SARS-CoV-2 via droplets and aerosols, Elife 10 (2021) e65774.
[8] V.C.C. Cheng, D.C. Lung, S.C. Wong, A.K.W. Au, Q. Wang, H. Chen, et al., Outbreak investigation of airborne transmission of Omicron (B. 1.1. 529)-SARS-CoV-2 variant of concern in a restaurant: implication for enhancement of indoor air dilution, J. Hazard. Mater. 430 (2022) 128504.
[9] P. Cheng, K. Luo, S. Xiao, H. Yang, J. Hang, C. Ou, et al., Predominant airborne transmission and insignificant fomite transmission of SARS-CoV-2 in a two-bus COVID-19 outbreak originating from the same pre-symptomatic index case, J. Hazard. Mater. 425 (2022) 128051.
[10] P. Cheng, W. Chen, S. Xiao, F. Xue, Q. Wang, P.W. Chan, et al., Probable cross-corridor transmission of SARS-CoV-2 due to cross airflows and its control, Build. Environ. 218 (2022) 109137.
[11] P. Cheng, W. Jia, L. Liu, H.L. Yen, Y. Li, What sizes of droplets contribute to long-range airborne transmission? Indoor Environ. (2024) 100045.
[12] C.A. Faulkner, T.I. Salsbury, B. Abboushi, C. Mouchref, B.C. Singer, M.D. Sohn, G. Arnold, Comparison of effectiveness and energy use of airborne pathogen mitigation measures to meet clean air targets in a prototypical office building, Build. Environ. 257 (2024) 111466.
[13] T.R. Frieden, C.T. Lee, Identifying and interrupting superspreading events—Implications for control of severe acute respiratory syndrome coronavirus 2, Emerg. Infect. Dis. 26 (6) (2020) 1059.
[14] W. Jia, P. Cheng, L. Ma, S. Wang, H. Qian, Y. Li, Individual heterogeneity and airborne infection: effect of non-uniform air distribution, Build. Environ. (2022) 109674.
[15] G. Johnson, L. Morawska, Z. Ristovski, M. Hargreaves, K. Mengersen, C.H. Chao, et al., Modality of human expired aerosol size distributions, J. Aerosol. Sci. 42 (12) (2011) 839–851.
[16] B. Jones, C. Iddon, M. Sherman, Quantifying quanta: determining emission rates from clinical data, Indoor Environ. 1 (3) (2024) 100025.
[17] Y. Li, X. Huang, I. Yu, T. Wong, H. Qian, Role of air distribution in SARS transmission during the largest nosocomial outbreak in Hong Kong, Indoor. Air. 15 (2) (2005) 83–95.
[18] Y. Li, G.M. Leung, J. Tang, X. Yang, C. Chao, J.Z. Lin, et al., Role of ventilation in airborne transmission of infectious agents in the built environment-a multidisciplinary systematic review, Indoor. Air. 17 (1) (2007) 2–18.
[19] J.O. Lloyd-Smith, S.J. Schreiber, P.E. Kopp, W.M. Getz, Superspreading and the effect of individual variation on disease emergence, Nature 438 (7066) (2005) 355–359.
[20] A.D. Luliano, K.M. Roguski, H.H. Chang, D.J. Muscatello, R. Palekar, S. Tempia, et al., Estimates of global seasonal influenza-associated respiratory mortality: a modelling study, Lancet 391 (10127) (2018) 1285–1300.
[21] Y. Li, H. Qian, J. Hang, X. Chen, P. Cheng, H. Ling, et al., Probable airborne transmission of SARS-CoV-2 in a poorly ventilated restaurant, Build. Environ. 196 (2021) 107788.
[22] Luo, D., Yong, W.H., Gao, C.X., Zheng, X., Li, Y., and Qian, H. (2024) What is an appropriate ventilation for public places during the COVID-19 pandemics. Submitted for publication.
[23] M. Marks, P. Millat-Martinez, D. Ouchi, C. h Roberts, A. Alemany, M. Corbacho-Monné, et al., Transmission of COVID-19 in 282 clusters in Catalonia, Spain: a cohort study, Lancet Infect. Dis. 21 (5) (2021) 629–636.
[24] M. Mitzenmacher, A brief history of generative models for power law and lognormal distributions, Internet. Math. 1 (2) (2004) 226–251.
[25] S.L. Miller, W.W. Nazaroff, J.L. Jimenez, A. Boerstra, G. Buonanno, S.J. Dancer, et al., Transmission of SARS-CoV-2 by inhalation of respiratory aerosol in the Skagit Valley Chorale superspreading event, Indoor. Air. 31 (2) (2021) 314–323.
[26] L. Morawska, J. Allen, W. Bahnfleth, P.M. Bluyssen, A. Boerstra, G. Buonanno, et al., A paradigm shift to combat indoor respiratory infection, Science (1979) 372 (6543) (2021) 689–691.
[27] E.A. Nardell, J. Keegan, S.A. Cheney, S.C. Etkind, Airborne infection. Theoretical limits of protection achievable by building ventilation, Am. Rev. Respir. Dis. 144 (2) (1991) 302–306.
[28] W.W. Nazaroff, Indoor aerosol science aspects of SARS-CoV-2 transmission, Indoor. Air. 32 (1) (2022) e12970.
[29] J. Neipel, J. Bauermann, S. Bo, T. Harmon, F. Jülicher, Power-law population heterogeneity governs epidemic waves, PLoS. One 15 (10) (2020) e0239678.
[30] C. Ou, S. Hu, K. Luo, H. Yang, J. Hang, P. Cheng, et al., Insufficient ventilation led to a probable long-range airborne transmission of SARS-CoV-2 on two buses, Build. Environ. 207 (2022) 108414.
[31] L.F. Pease, T.I. Salsbury, K. Anderson, R.M. Underhill, J.E. Flaherty, A. Vlachokostas, et al., Size dependent infectivity of SARS-CoV-2 via respiratory droplets spread through central ventilation systems, Int. Commun. Heat Mass Transf. 132 (2022) 105748.
[32] O. Puhach, K. Adea, N. Hulo, P. Sattonnet, C. Genecand, A. Iten, et al., Infectious viral load in unvaccinated and vaccinated individuals infected with ancestral, Delta or Omicron SARS-CoV-2, Nat. Med. 28 (7) (2022) 1491–1500.
[33] H. Qian, T. Miao, L. Liu, X. Zheng, D. Luo, Y. Li, Indoor transmission of SARS-CoV-2, Indoor. Air. 31 (3) (2021) 639–645.
[34] S.N. Rudnick, D.K. Milton, Risk of indoor airborne infection transmission estimated from carbon dioxide concentration, Indoor. Air. 3 (3) (2003) 237–245.
[35] C.E. Troeger, B.F. Blacker, I.A. Khalil, S.R. Zimsen, S.B. Albertson, D. Abate, et al., Mortality, morbidity, and hospitalisations due to influenza lower respiratory tract infections, 2017: an analysis for the Global Burden of Disease Study 2017, Lancet Respir. Med. 7 (1) (2019) 69–89.
[36] D. Vernez, S. Schwarz, J.J. Sauvain, C. Petignat, G. Suarez, Probable aerosol transmission of SARS-CoV-2 in a poorly ventilated courtroom, Indoor. Air. 31 (6) (2021) 1776–1785.
[37] A. Vlachokostas, C.A. Burns, T.I. Salsbury, R.C. Daniel, D.P. James, J.E. Flaherty, et al., Experimental evaluation of respiratory droplet spread to rooms connected by a central ventilation system, Indoor. Air. 32 (1) (2022) e12940.
[38] B.C. Wong, N. Lee, Y. Li, P.K. Chan, H. Qiu, Z. Luo, et al., Possible role of aerosol transmission in a hospital outbreak of influenza, Clin. Infectious Dis. 51 (10) (2010) 1176–1183.
[39] WHO. (2020). The top 10 causes of death. https://www.who.int/news-room/fact-sheets/detail/the-top-10-causes-of-death. Accessed on 11/07/2024.
[40] C.C. Wang, K.A. Prather, J. Sznitman, J.L. Jimenez, S.S. Lakdawala, Z. Tufekci, et al., Airborne transmission of respiratory viruses, Science (1979) 373 (6558) (2021) eabd9149.
[41] S. Xiao, Y. Li, M. Sung, J. Wei, Z. Yang, A study of the probable transmission routes of MERS-CoV during the first hospital outbreak in the Republic of Korea, Indoor. Air. 28 (1) (2018) 51–63.
[42] Y. Guo, Z. Dou, N. Zhang, X. Liu, B. Su, Y. Li, Y. Zhang, Student close contact behavior and COVID-19 transmission in China's classrooms, PNAS. Nexus. 2 (5) (2023) pgad142.